Supplementary Material

Paper: Organic molecular markers and signature from wood combustion particles in winter ambient aerosols: Aerosol mass spectrometer (AMS) and high time-resolved GC-MS measurements in Augsburg, Germany

SI-1 Collection efficiency

The collection efficiency describes the transmission of the particle through the aerodynamic lens, the focus on and arrival at the vaporiser of the particle, and the vaporisation of the non-refractory compounds. One of the most problematic parts is the particle bounce at the vaporiser. The particle bounce off the vaporiser without vaporisation and therefore without detection of these particles (bounce efficiency) (Huffman et al., 2005). One way to estimate the CE is to compare the AMS results with other instruments. The AMS data were compared to the SMPS data on the basis of the total volume of the particles. This provides a CE around 0.6 (Figure SI-1.3). Comparisons of the total mass or specific compound mass with other instruments, such as a tapered element oscillating microbalance (TEOM) or a sulfate particulate monitor, estimate a CE of 0.4 (Figure SI-1.2). Both the SO4 monitor and TEOM measure $PM_{2.5}$ and this may be the cause of the difference. However, the CE estimation on this way is difficult, which is due to the individual uncertainties and different PM size ranges of these instruments.

Another possibility is to use the typical AMS CE of 0.5 and to define the bounce efficiency (E_b). This bounce efficiency depends on the water and nitrate content of the particles. Therefore, it is necessary to estimate the nitrate dependence (Figure SI-1.2 and SI-1.3) and the acidity balance (Figure SI-1.1). If particles are not neutralized (acidity balance), they are more likely to be liquid and less likely to bounce. Without nitrate dependence and balanced acidity, a CE of 0.5 is acceptable, even when typical CE uncertainty suggests that CE can vary by around 20% (Bahreini et al., 2009).

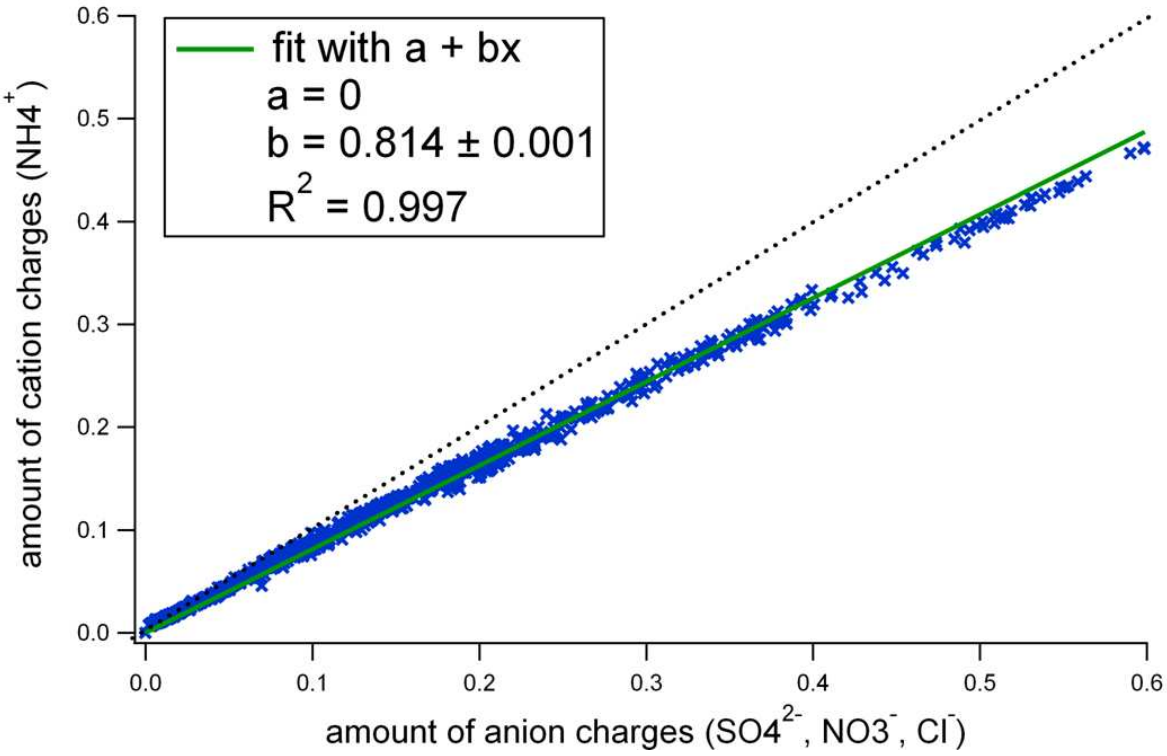

Figure SI-1.1: The y-axes represent the amount of positive charges from ammonium cation and the x-axes represent the sum of all negative charges from the anions sulphate, nitrate and chloride. The slope calculated with the orthogonal distance regression lies not completely on the 1 to 1 line, but in a reasonable range. The RIE for ammonium was 3.96 during the IE calibration and that value is applied in the data analysis program.

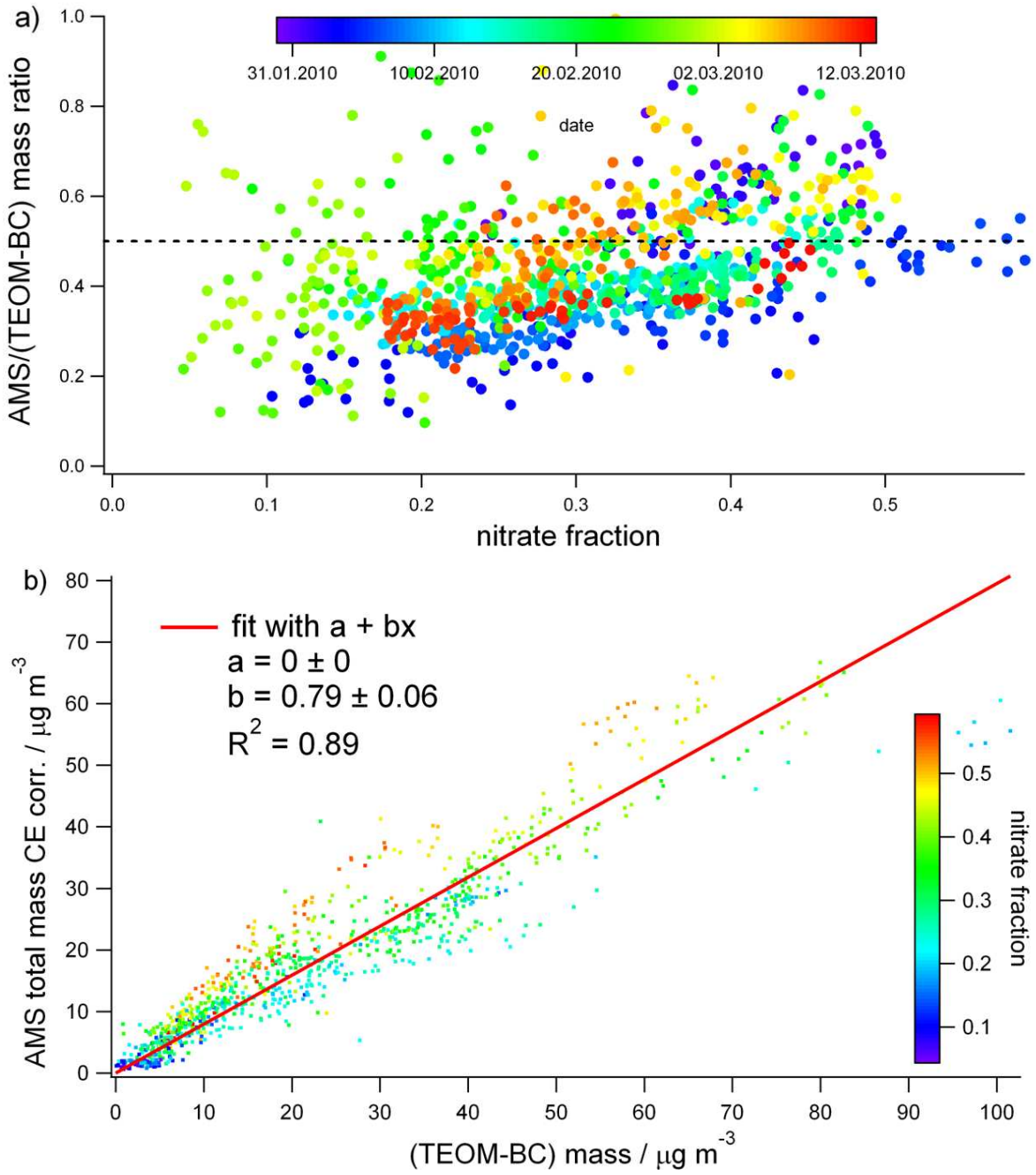

Figure SI-1.2: a) The ratio of the total AMS mass (sum of all compounds) and the $PM_{2.5}$ mass concentration from the TEOM subtracted by the BC mass of the Aethalometer amounts to approximately 0.4, which is probably due to the lower PM size cut of the AMS. b) Scatter plot of the CE (CE = 0.5) corrected AMS total mass versus the $PM_{2.5}$ mass concentration from the TEOM subtracted by the BC mass colored by the nitrate fraction. Regression values are calculated with the orthogonal distance regression with a correlation of R^2 = 0.85. The slope also provides a lower mass for the AMS results similar to Figure a. The comparison between this ratio and the nitrate fraction (Figure a) and colored data points in Figure b indicates a nitrate dependence of the E_b for data points with higher nitrate fractions.

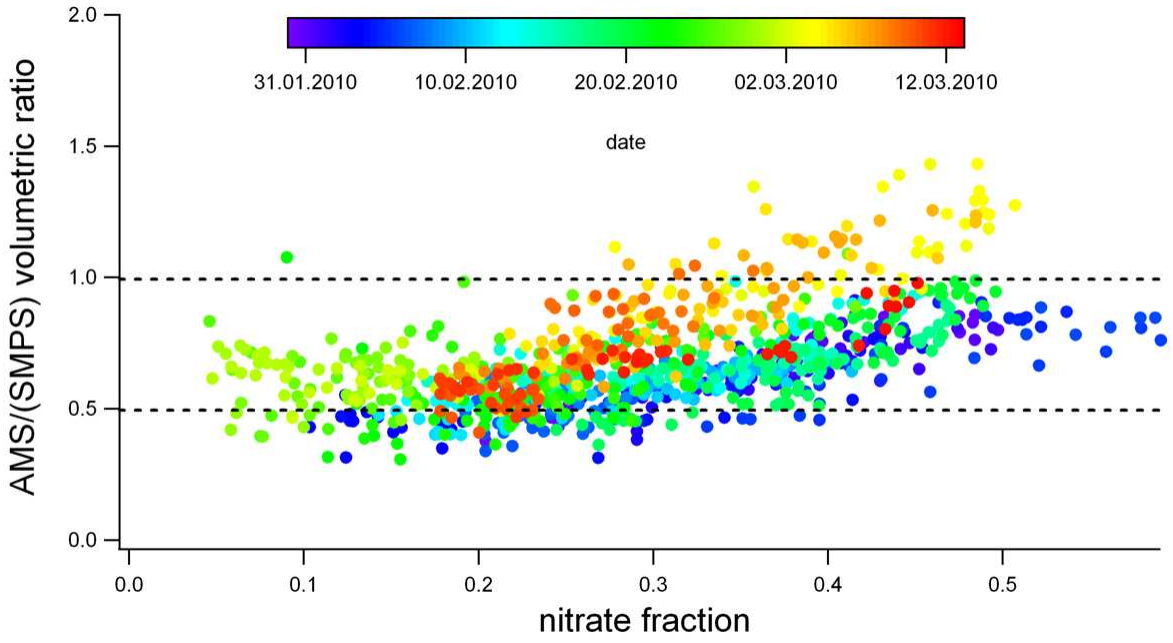

Figure SI-1.3: The volumetric ratio of the total volume of the AMS species and total particle volume of the SMPS data amounts to approximately 0.6. The AMS total was calculated from the different AMS species masses and their densities. The size range of the SMPS data was from 50 to 1000 nm (for details see Pitz et al. 2008). AS in Figure SI-1-2 this volumetric ratio shows a nitrate dependence of the E_b.

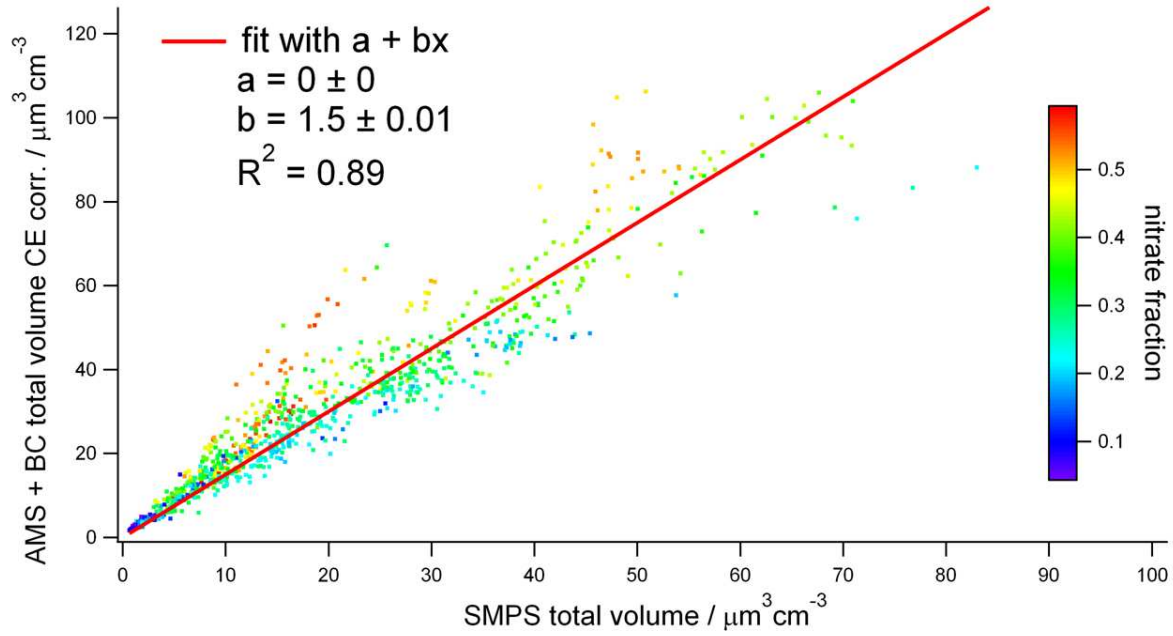

Figure SI-1.4: Scatter plot of the total volume from the CE (CE = 0.5) corrected AMS species and BC compared to the total particle volume of the SMPS data colored by the nitrate fraction. Regression values are calculated with the orthogonal distance regression with a correlation of $R^2 = 0.89$ and slope of 1.5.

To see how much the nitrate dependence affects the CE and the measurement results, we compared the AMS results with a CE of 0.5 with AMS results calculated with an alternated CE in Figure SI-1.5. This alternated CE takes high nitrate fraction into account and is obtained with a new calculation, following Middlebrook et al. (2012):

$$CE = \max(0.45,\ 0.0833 + 0.9167 \cdot ANMF)\,, \qquad \text{(SI-1)}$$

where ANMF is the ammonium nitrate mass fraction:

$$ANMF = \frac{80/62 \cdot NO_3^-}{NH_4^+ + SO_4^{2-} + NO_3^- + Cl^- + Org}\,. \qquad \text{(SI-2)}$$

If the ANMF is below 0.4, the CE is set to a constant CE of 0.45, otherwise the CE has a linear dependence, which follows the calculation (SI-1).

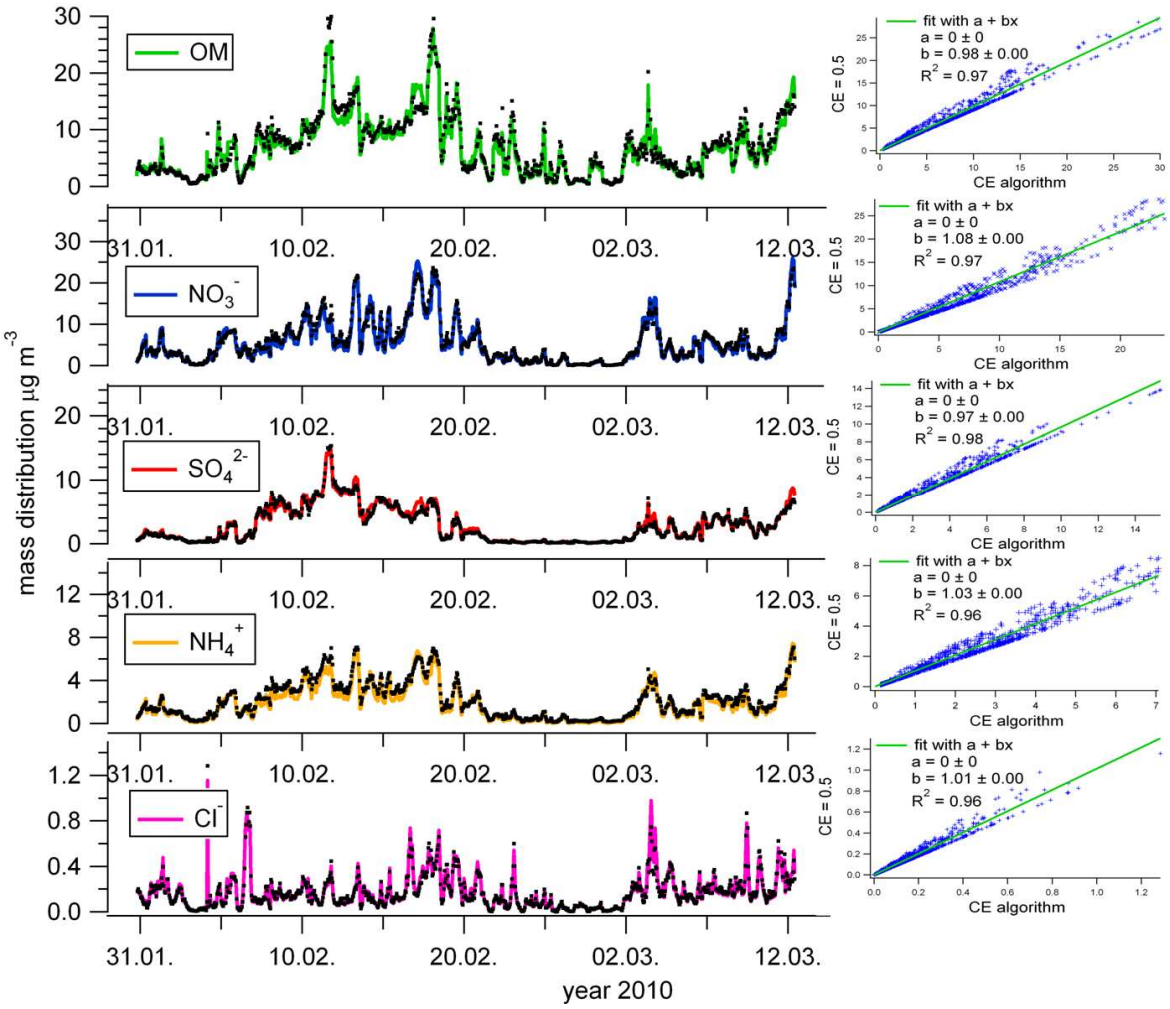

Figure SI-1.5: Individual time series of the organic (green), nitrate (blue), sulphate (red), ammonium (orange) and chloride (pink) with a CE of 0.5 and with the calculated CE algorithms (black dots) measured by the AMS. On the left site of the figure, the different time series for each fraction shows a good agreement (R^2 = 0.96-98).

55% of the obtained AMNP values are more below 0.4, resulting that the CE is set to 0.45 instead of the constant CE of 0.5. Additionally, with this calculation 67% of the data points are below a CE of 0.5. However, the ratios and comparisons in Figure SI-1.3 and SI-1-4 suggest a higher CE. Due to this and the fact that the nitrate dependence take not so much into account in the obtained results (Figure S1-5), we use the constant CE of 0.5 and refer that uncertainty CE during field missions can be on the order of 20% (Bahreini et al., 2009).

SI-2 PMF

SI-2.1 Three Factor PMF solution

The choice of the three-factor solution is confirmed by looking at the *Q/Qexpected* versus the number of factors Figure SI-2.1.

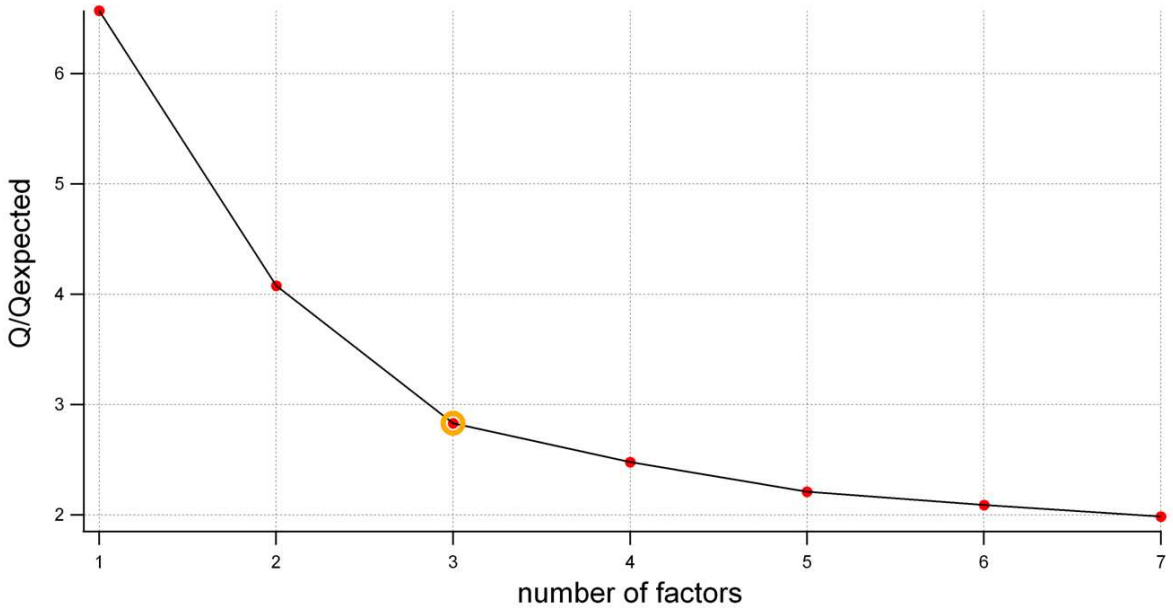

Figure SI-2.1: *Q/Qexpected* value dependence of the numbers of PMF factors with the chosen third factor. A large drop in the *Q/Qexpected* value is shown increasing the number of factors until three; the addition of more factors does not significantly change the slope of the curve.

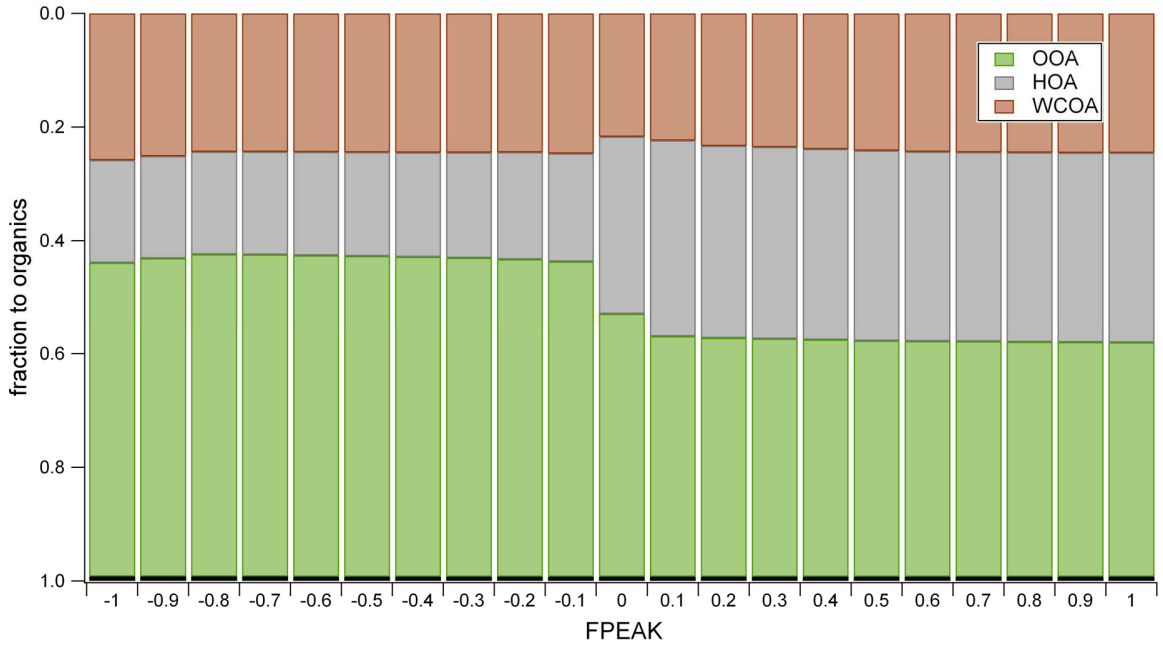

Figure SI-2.2: OOA (green), HOA (grey) and WCOA (brown) fraction of total organics in dependence on the FPEAKs. HOA and OOA change their impact from the negative to the positive FPEAK range.

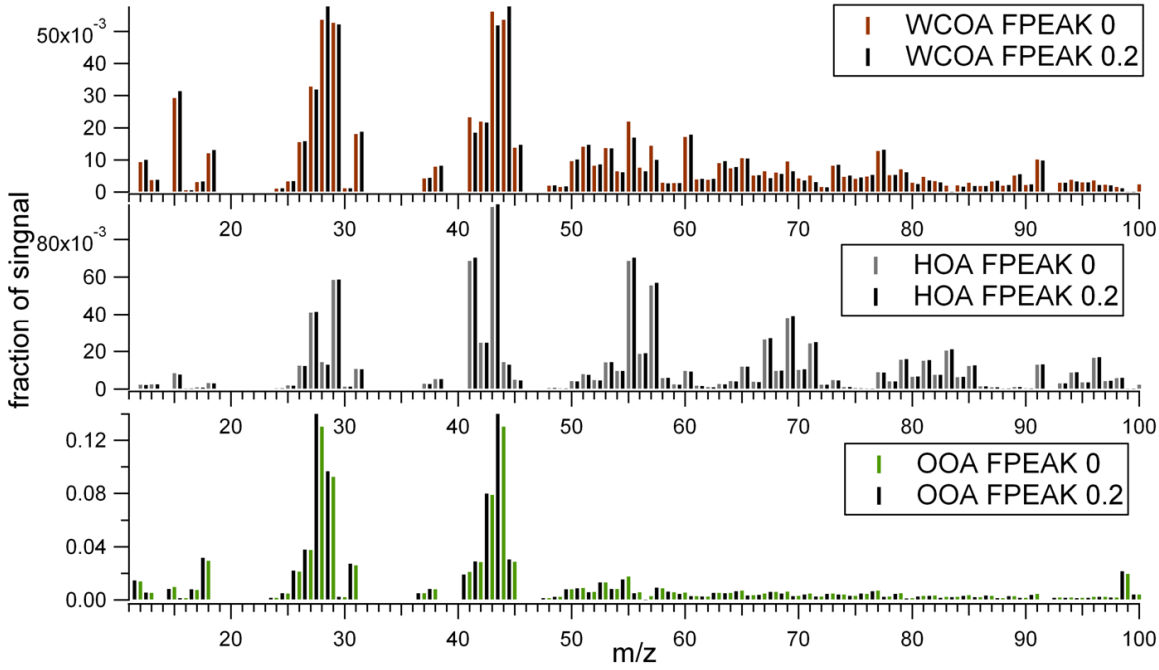

Figure SI-2.3: Comparison of PMF mass spectra from WCOA (brown), HOA (grey) and OOA (green) considering FPEAK 0 and 0.2. Both the mass spectra and time series do not show significant changes when considering FPEAK 0 and FPEAK 0.2.

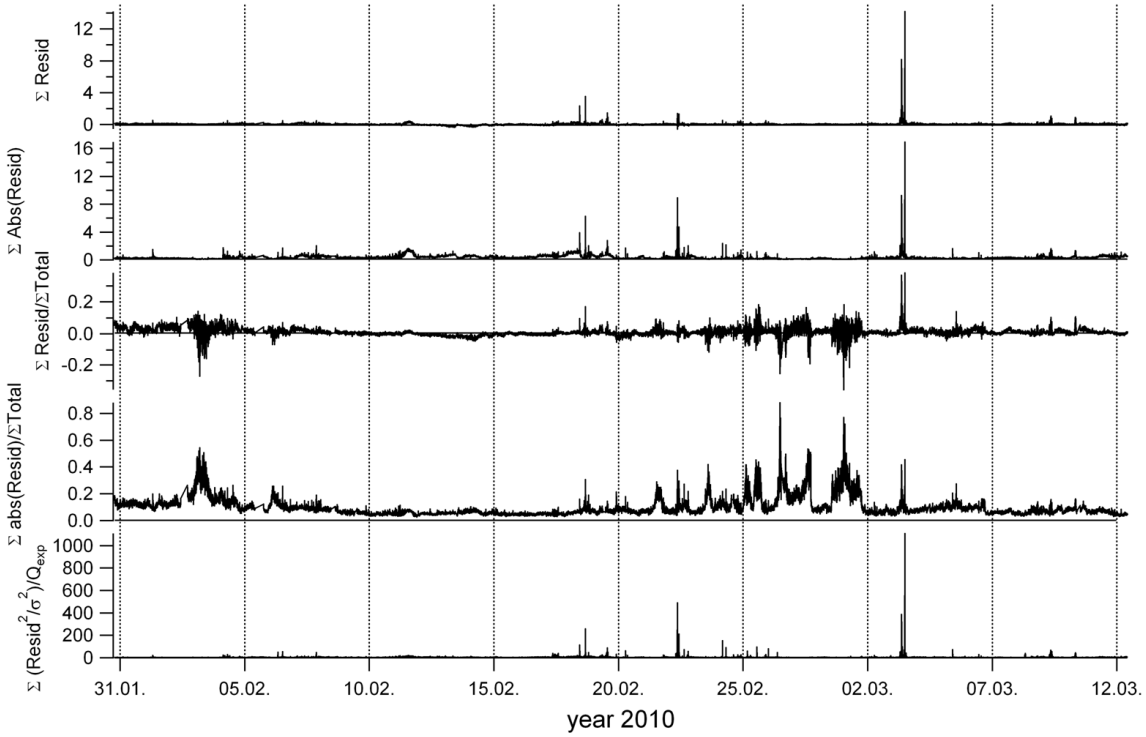

Figure SI-2.4: Residual of the time series from the three-factor PMF solution at FPEAK 0.2 over the whole measurement period. In periods with low PM and the special snow event at 03 March 2010 provide higher residuals.

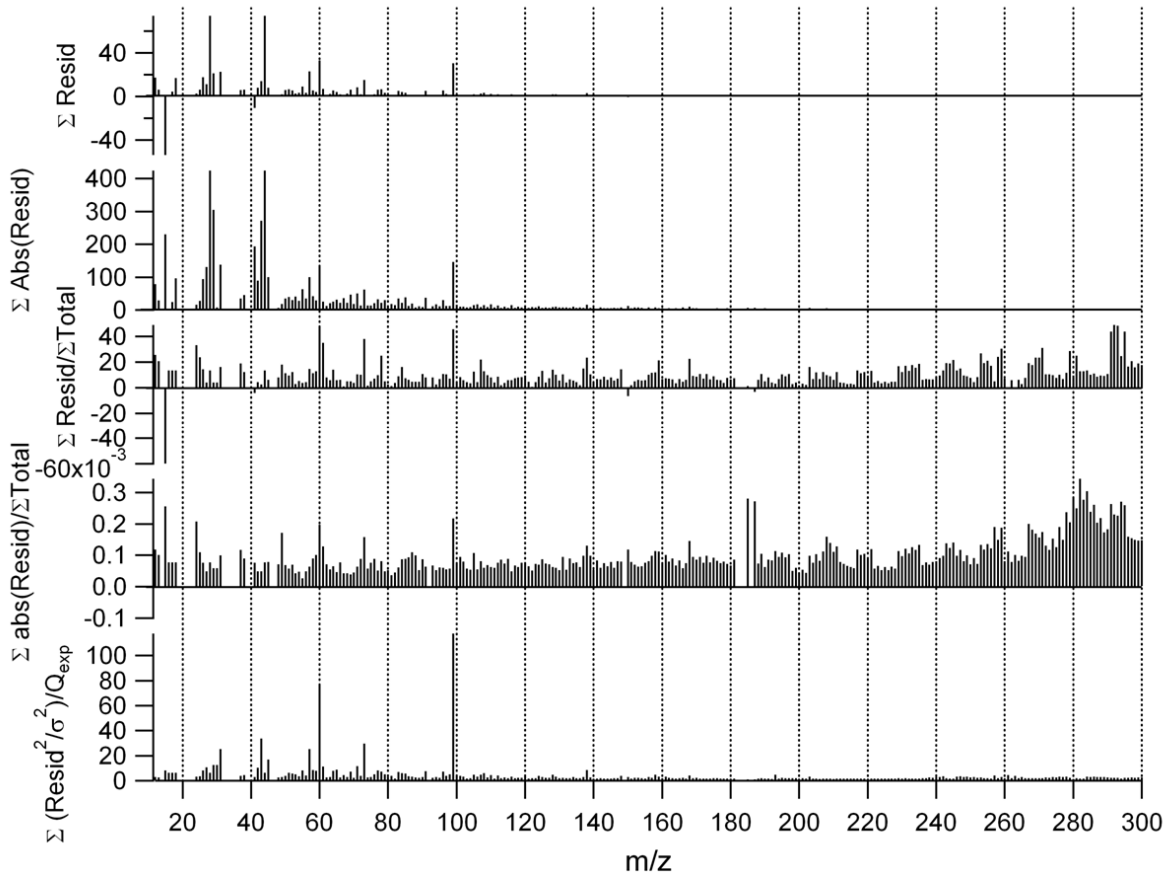

Figure SI-2.5: Residual of the mass spectra from the three-factor PMF solution at FPEAK 0.2 over the whole measurement period. The signal at m/z 99 has high residuals; however, it has higher concentration than the neighbour m/z signals. Additionally, it is estimated with the additional AMS and PMF analysis from the mobile laboratory (MOSQUITA) measurements. Hence it is important to take the signal at m/z 99 also into account for the PMF analysis.

SI-2.2 Four Factor PMF solution

AMS PMF results of the four-factor PMF solution during the measurement period from 31 January to 12 March, with FPEAK = 0.

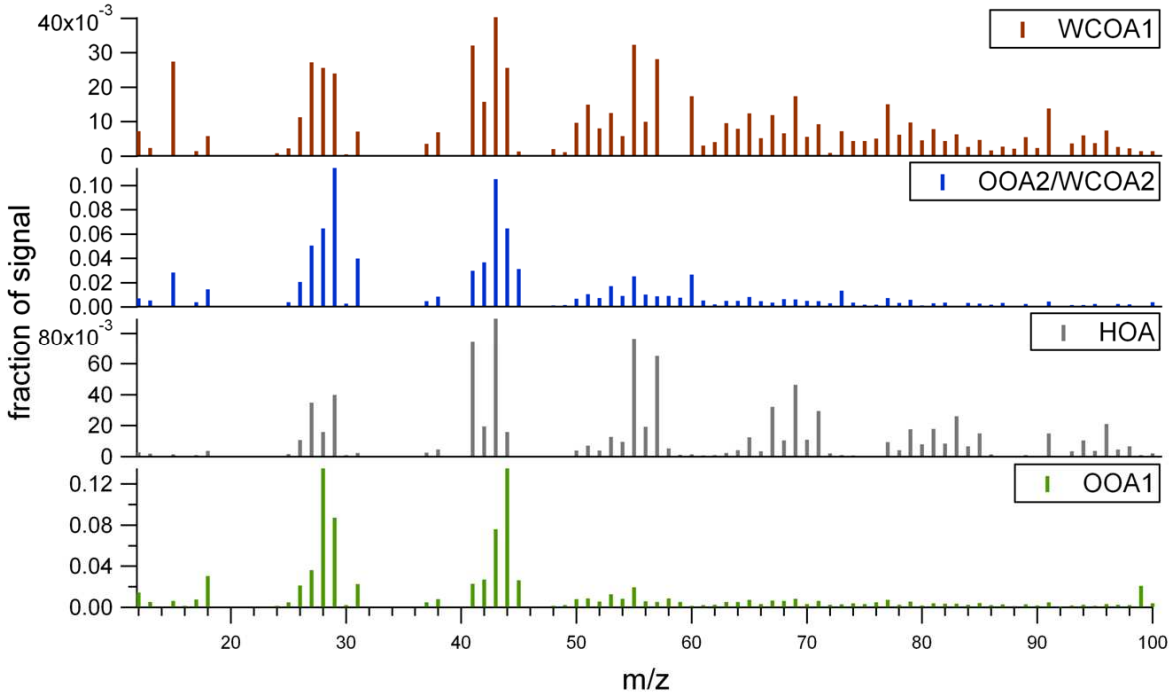

Figure SI-2.6: (a) Calculated mass spectra of the four PMF factors solution with OOA1 (green), HOA (grey) OOA2/WCOA2 (blue) and WCOA1 (brown).

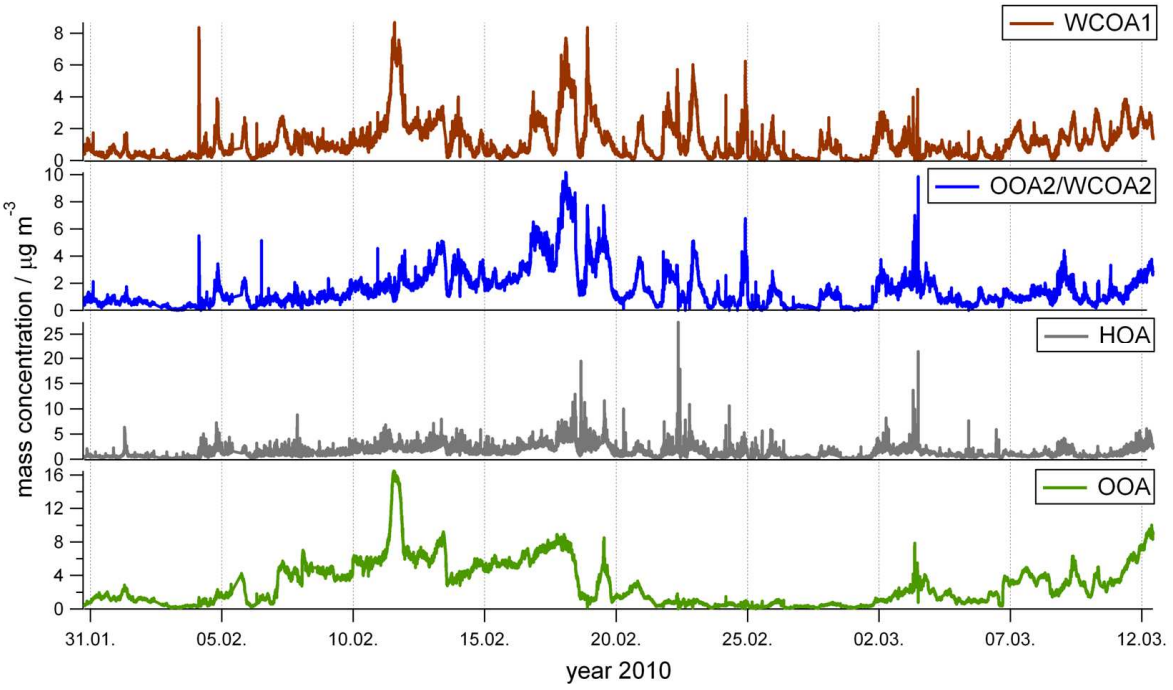

Figure SI-2.7: Time series of the four PMF factors: OOA1 (green), HOA (grey) OOA2/WCOA2 (blue) and WCOA1 (brown).

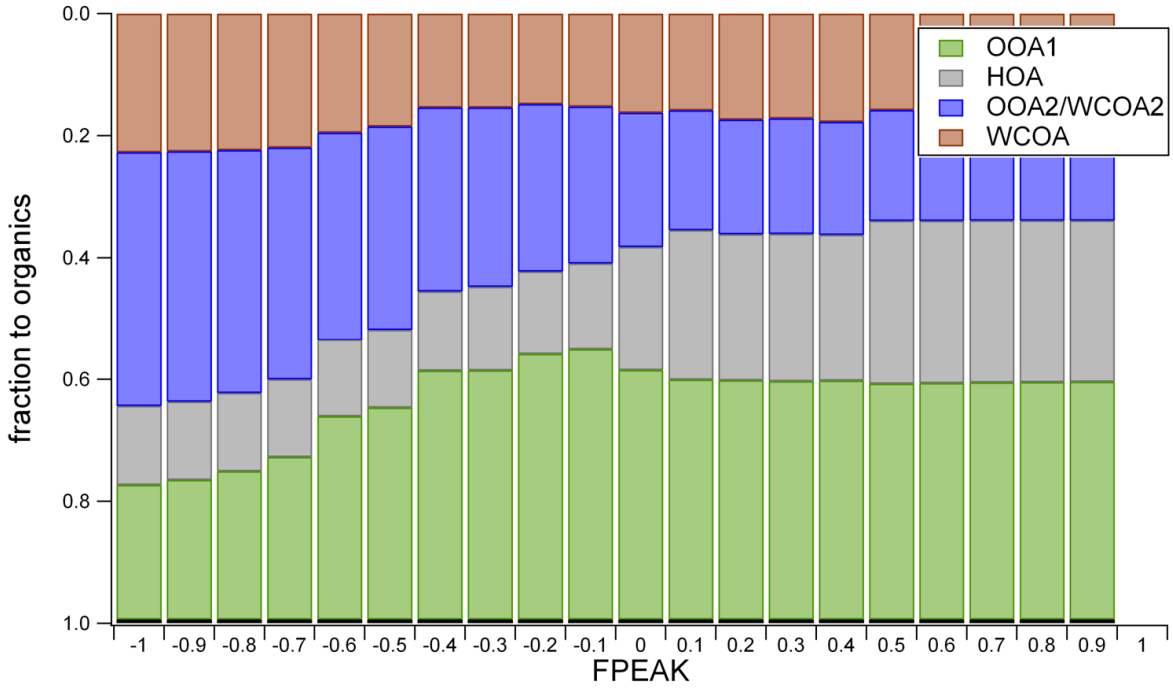

Figure SI-2.8: OOA1 (green), HOA (grey) OOA2/WCOA2 (blue) and WCOA1 (brown) fraction of total organics in dependence on the FPEAKs. HOA and OOA change their impact from the negative to the positive FPEAK range. Over positive FPAEK the PMF solutions are stable; during the negative FPEAKs the second secondary factor (OOA2/WCOA2) take more parts from the OOA1.

SI-3 Graphs for Results and Discussion

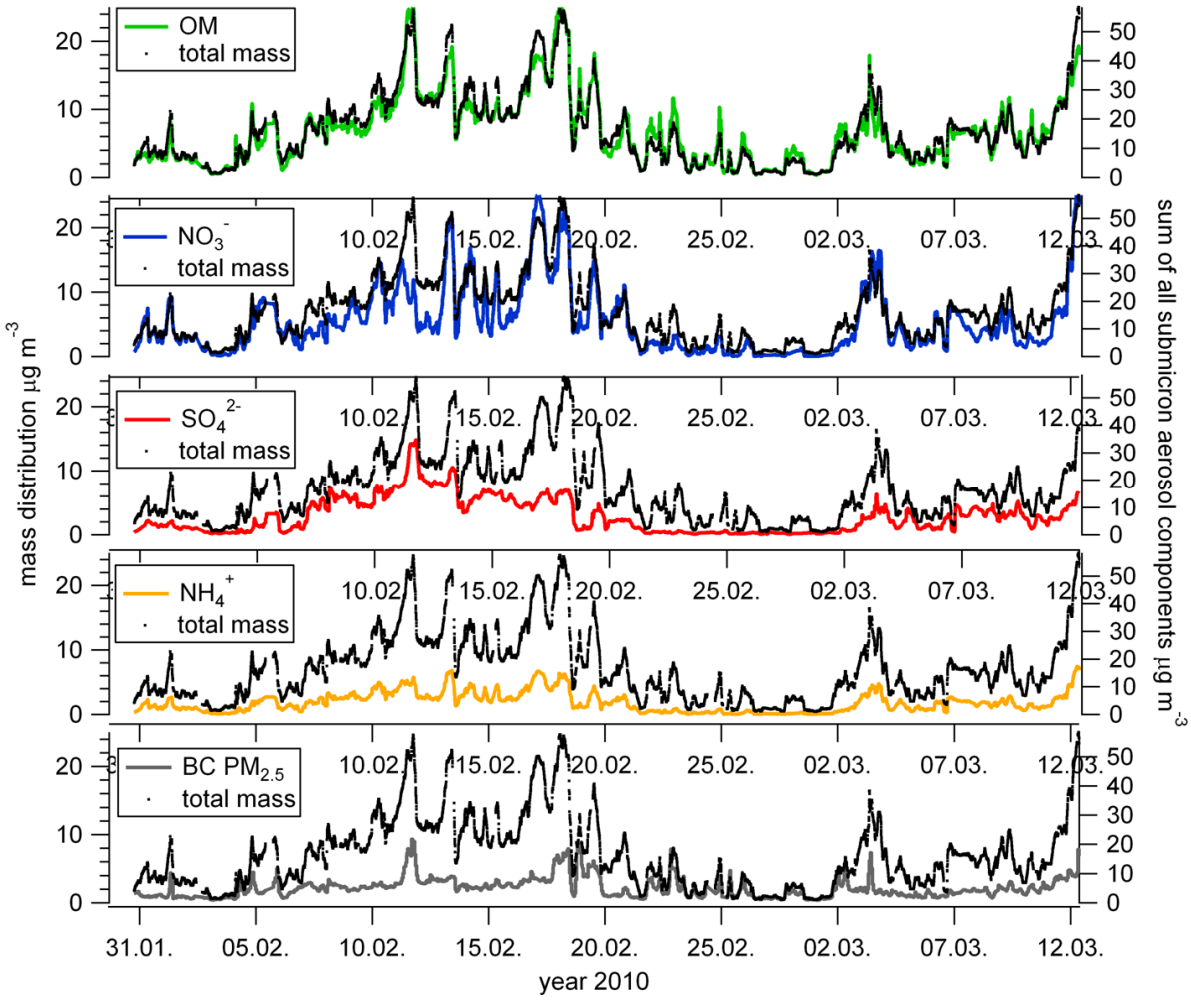

Figure SI-3.1: Hourly mean time series of submicron aerosol components with the AMS organic (green), nitrate (blue), sulphate (red), ammonium (orange) and the $PM_{2.5}$ BC (grey) from the Aethalometer data. The sum of all these submicron aerosol components (black dots) is plotted on the right axis.

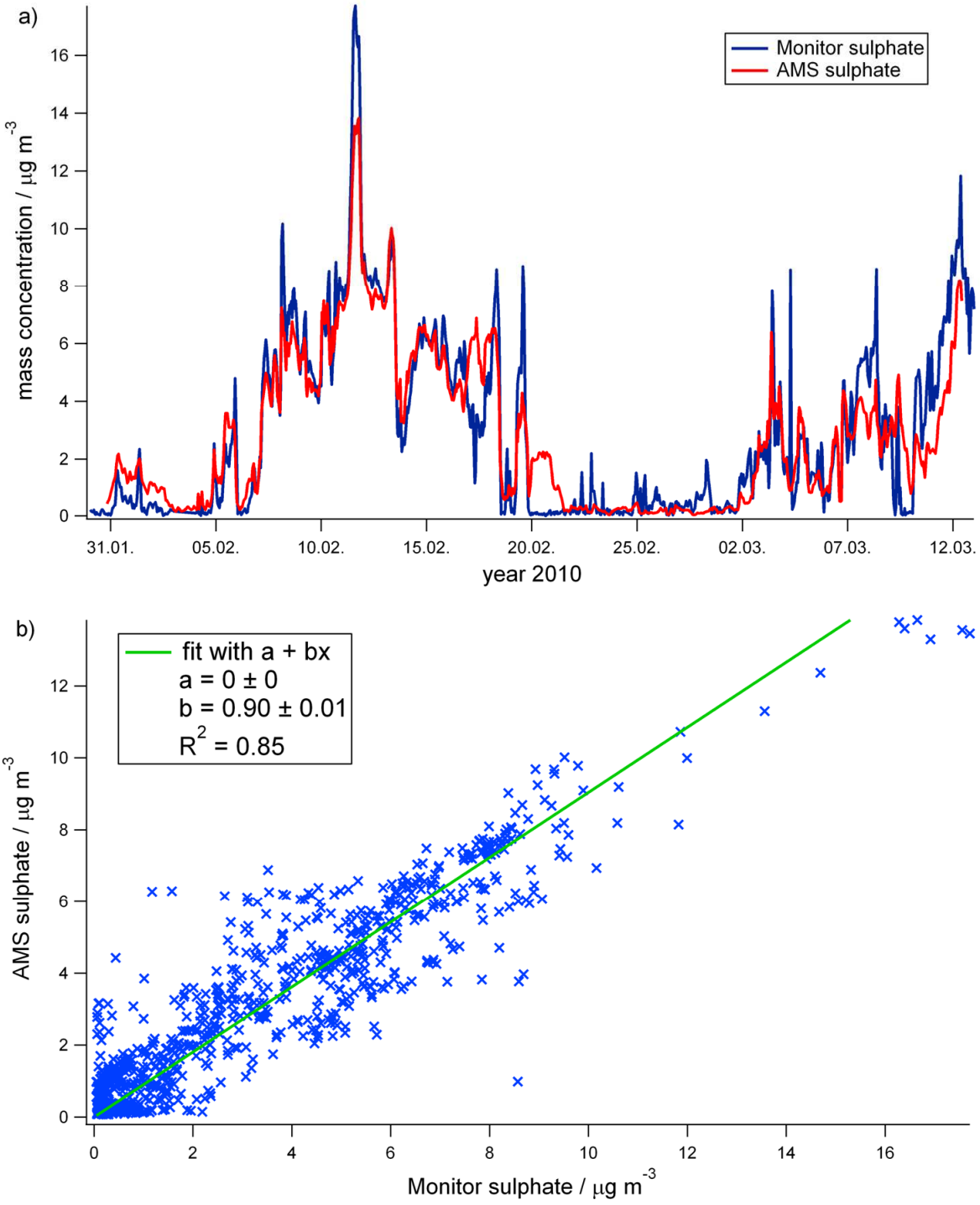

Figure SI-3.2: (a) Sulphate concentration correlation during the campaign from sulphate of the AMS (red) with a CE of 0.5 and sulphate particulate monitor measurements (blue). (b) Scatter plot of hourly mean sulphate concentration of the AMS versus sulphate particulate monitor measurements. Regression values are calculated with the orthogonal distance regression. The two time series give a correlation R^2 of 0.85. The slope below one is probably due to the higher size cut of $PM_{2.5}$ from the sulphate monitor.

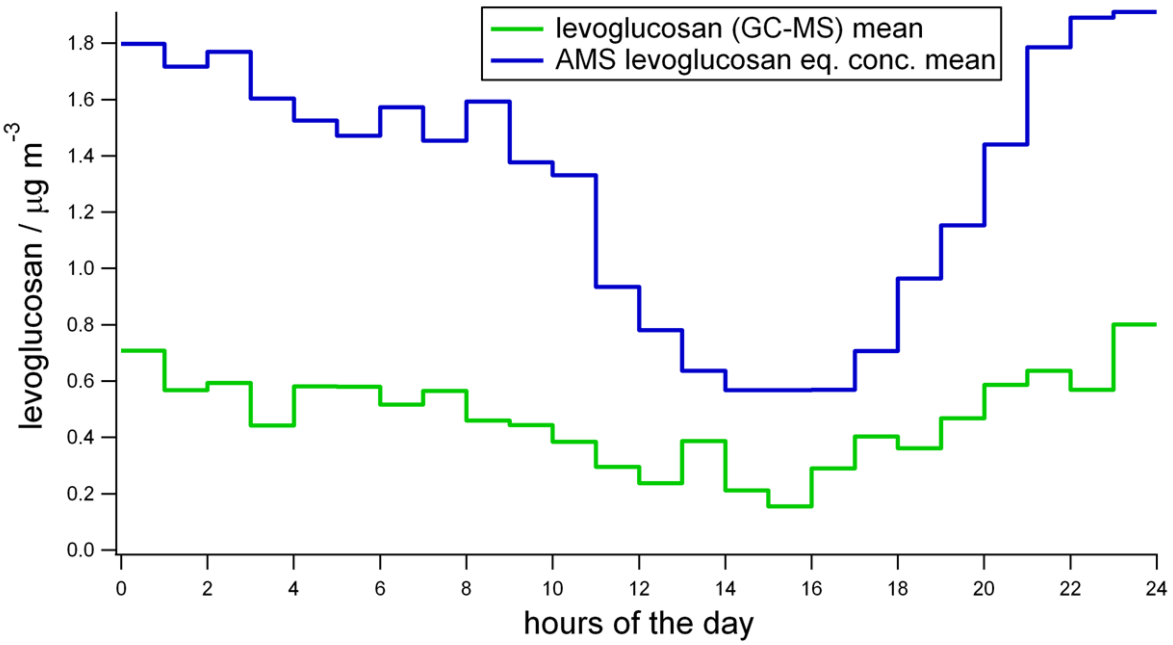

Figure SI-3.3: Diurnal variation of PM_1 filter levoglucosan concentration of the GC-MS measurements (green) and of AMS levoglucosan equivalent concentration calculated over 87 data points during the PM_1 filter period. The spiky variation is due to the low number of data points. However the diurnal variation of AMS levoglucosan equivalent concentration shows a longer morning emission period.

Table SI-1: Correlation factor R^2 of the four source factors from the four-factor solution with the marker ion at signal m/z 44, 57, and 60, as well as with the AMS sulphate, nitrate, ammonium, $PM_{2.5}$ Aethalometer BC, and hourly PM_1 levoglucosan GC-MS data.

	OOA1	**HOA**	**OOA2/WCOA2**	**WCOA**
SO_4	0.38	**0.89**	0.19	0.22
NH_4	0.38	**0.73**	0.45	0.40
NO_3	0.30	0.53	0.53	0.43
BC	0.43	0.44	0.50	0.71
PM_1 GC-MS levoglucosan	0.28	0.01	**0.73**	0.45
m/z 44	0.43	**0.93**	0.49	0.47
m/z 57	0.46	0.43	0.72	0.93
m/z 60	0.40	0.37	**0.86**	0.70

References

Bahreini, R., Ervens, B., Middlebrook, A.M., Warneke, C., de Gouw, J.A., DeCarlo, P.F., Jimenez, J.L., Atlas, E., Brioude, J., Brock, C.A., Fried, A., Holloway, J.S., Peischl, J., Richter, D., Ryerson, T.B., Stark, H., Walega, J., Weibring, P., Wollny, A.G., Fehsenfeld, F.C.: Organic Aerosol Formation in Urban and Industrial plumes near Houston and Dallas, TX, J. Geophys. Res., 114, D00F16, 2009.

Huffman, J.A., Jayne, J.T., Drewnick, F., Aiken, A.C., Onasch, T., Worsnop, D.R., and Jimenez, J.L.: Design, Modeling, Optimization, and Experimental Tests of a Particle Beam Width Probe for the Aerodyne Aerosol Mass Spectrometer, Aerosol Sci. Technol., 39, 1143-1163, DOI:10.1080/02786820500423782, 2005.

Middlebrook, A.M., Bahreini, R., Jimenez, J.L., and Canagaratna, M.R.: Evaluation of Composition-Dependent Collection Efficiencies for the Aerodyne Aerosol Mass Spectrometer using Field Data, Aerosol Sci. Technol., 46, 258–271, DOI:10.1080/02786826.2011.620041, 2012.

Pitz, M., Birmili, W., Schmid, O., Peters, A., Wichmann, H. E., and Cyrys, J.: Quality control and quality assurance for particle size distribution measurements at an urban monitoring station in Augsburg, Germany. J Environ Monitor, 10(9), 1017-1024, 2008.